# Molecular Characterization of Acquired Resistance to KRAS$^{G12C}$–EGFR Inhibition in Colorectal Cancer

Rona Yaeger[1], Riccardo Mezzadra[2], Jenna Sinopoli[1], Yu Bian[1], Michelangelo Marasco[3], Esther Kaplun[3], Yijun Gao[3], HuiYong Zhao[4], Arnaud Da Cruz Paula[5], Yingjie Zhu[5], Almudena Chaves Perez[2], Kalyani Chadalavada[6], Edison Tse[7], Sudhir Chowdhry[7], Sydney Bowker[4], Qing Chang[4], Besnik Qeriqi[4], Britta Weigelt[5], Gouri J. Nanjangud[6], Michael F. Berger[5,8], Hirak Der-Torossian[9], Kenna Anderes[9], Nicholas D. Socci[8], Jinru Shia[5], Gregory J. Riely[1], Yonina R. Murciano-Goroff[1], Bob T. Li[1,10], James G. Christensen[9], Jorge S. Reis-Filho[5], David B. Solit[1,8], Elisa de Stanchina[4], Scott W. Lowe[2,11], Neal Rosen[1,3,12], and Sandra Misale[3]

## ABSTRACT

With the combination of KRAS$^{G12C}$ and EGFR inhibitors, KRAS is becoming a druggable target in colorectal cancer. However, secondary resistance limits its efficacy. Using cell lines, patient-derived xenografts, and patient samples, we detected a heterogeneous pattern of putative resistance alterations expected primarily to prevent inhibition of ERK signaling by drugs at progression. Serial analysis of patient blood samples on treatment demonstrates that most of these alterations are detected at a low frequency except for *KRAS*$^{G12C}$ amplification, a recurrent resistance mechanism that rises in step with clinical progression. Upon drug withdrawal, resistant cells with *KRAS*$^{G12C}$ amplification undergo oncogene-induced senescence, and progressing patients experience a rapid fall in levels of this alteration in circulating DNA. In this new state, drug resumption is ineffective as mTOR signaling is elevated. However, our work exposes a potential therapeutic vulnerability, whereby therapies that target the senescence response may overcome acquired resistance.

**SIGNIFICANCE:** Clinical resistance to KRAS$^{G12C}$–EGFR inhibition primarily prevents suppression of ERK signaling. Most resistance mechanisms are subclonal, whereas *KRAS*$^{G12C}$ amplification rises over time to drive a higher portion of resistance. This recurrent resistance mechanism leads to oncogene-induced senescence upon drug withdrawal and creates a potential vulnerability to senolytic approaches.

## INTRODUCTION

*KRAS* is the most mutated oncogene in human cancer (1). It acts as a signaling switch that, when bound to GTP, orchestrates a program of cell proliferation and survival. Until recently, efforts to target KRAS have been unsuccessful due to its small binding pocket, high affinity for GTP, and redundant mechanisms of posttranslational processing. The development of allele-specific KRAS$^{G12C}$ inhibitors that trap KRAS in the inactive, GDP-bound state (2, 3) led to a paradigm change, with clinical responses in 30% to 50% of patients with non–small cell lung cancer (NSCLC) harboring KRAS$^{G12C}$ mutations (4, 5).

[1]Department of Medicine, Memorial Sloan Kettering Cancer Center, New York, New York. [2]Department of Cancer Biology and Genetics, Memorial Sloan Kettering Cancer Center, New York, New York. [3]Molecular Pharmacology Program, Memorial Sloan Kettering Cancer Center, New York, New York. [4]Antitumour Assessment Core Facility, Memorial Sloan Kettering Cancer Center, New York, New York. [5]Department of Pathology, Memorial Sloan Kettering Cancer Center, New York, New York. [6]Molecular Cytogenetics Core Facility, Memorial Sloan Kettering Cancer Center, New York, New York. [7]Boundless Bio, Inc., San Diego, California. [8]Kravis Center for Molecular Oncology, Memorial Sloan Kettering Cancer Center, New York, New York. [9]Mirati Therapeutics, Inc., San Diego, California. [10]Weill Cornell Medical College, New York, New York. [11]Howard Hughes Medical Institute, Chevy Chase, Maryland. [12]Center for Molecular-Based Therapy, Memorial Sloan Kettering Cancer Center, New York, New York.

**Corresponding Authors:** Rona Yaeger, Department of Medicine, Memorial Sloan Kettering Cancer Center, New York, NY 10065. Phone: 646-888-5109; E-mail: yaegerr@mskcc.org; and Sandra Misale, Molecular Pharmacology Program, Memorial Sloan Kettering Cancer Center, New York, NY 10065. Phone: 646-888-2076; E-mail: misales@mskcc.org

Cancer Discov 2023;13:41–55

**doi:** 10.1158/2159-8290.CD-22-0405

These agents are not as effective in colorectal cancers with KRAS$^{G12C}$ mutation. We have previously shown that the activity of these drugs in KRAS$^{G12C}$ colorectal cancer is limited because activation of epidermal growth factor receptor (EGFR) reactivates ERK signaling and consequently combinatorial KRAS$^{G12C}$ and EGFR inhibition more effectively targets KRAS$^{G12C}$ colorectal cancer (6). Early trial data provide clinical support for this observation: The response rate for sotorasib was 7% to 10% in colorectal cancer (7), and, in the first report of sotorasib plus the EGFR antibody panitumumab, the response rate was 27% (8). For adagrasib monotherapy, it was ~20%, and, for adagrasib with the EGFR antibody cetuximab, it increased to ~40% (9). Based on these data, combination treatments based on KRAS$^{G12C}$ inhibitors and EGFR antibodies are being evaluated in registrational, phase III trials.

Nonetheless, patients treated with these agents eventually acquire resistance, and the response to single-agent or combination treatment is brief. Several studies have characterized resistance to KRAS$^{G12C}$ monotherapy (10–12). Remarkably, these alterations are highly heterogeneous, including KRAS, BRAF, or MEK mutations, as well as gene amplifications and fusions, and circulating tumor DNA (ctDNA) analysis typically identifies multiple resistance alterations in the same patient. Here, we sought to determine the landscape of genetic mechanisms of resistance to EGFR–KRAS$^{G12C}$ inhibition in gastrointestinal cancer and to identify novel approaches to potentially overcome resistance.

## RESULTS

### Mechanisms of Resistance to Combined KRAS$^{G12C}$ and EGFR Inhibition

To identify mechanisms of resistance to the combination of KRAS$^{G12C}$ and EGFR inhibitors, we grew the colorectal cancer cell lines C106 and RW7213, both of which are sensitive to this treatment (6), in drugs until the emergence of secondary resistance (Fig. 1A). Treatment with 3 μmol/L sotorasib and 50 μg/mL cetuximab led to massive cell death of both cell lines with few viable cells. Cells were therefore subjected to increasing doses of sotorasib (from 0.1 to 3 μmol/L) with 50 μg/mL cetuximab to generate resistance (Supplementary Fig. S1A). Resistant sublines grew well in drugs after a period of 4 months for C106 cells and 2 months for RW7213 cells (Supplementary Fig. S1A–S1C).

Both resistant sublines expressed higher RAS-GTP levels than parental cells, and drug treatment led to incomplete inhibition of RAS-GTP (Supplementary Fig. S1D and S1E). Drug treatment of C106-resistant cells failed to suppress activity of downstream effectors in the RAS/ERK pathway, whereas RW7213 resistant cells experienced a reduction in pathway activity but continued to have high levels of p-MEK and p-ERK due to elevated baseline pathway activation. Targeted sequencing of the resistant sublines using MSK-IMPACT (13) identified acquired clonal *NRAS*$^{G12D}$ mutation and subclonal *APC*$^{Q879*}$ nonsense mutation in C106-resistant cells and amplification of *KRAS*$^{G12C}$ in RW7213 resistant cells, which have a homozygous (through loss of heterozygosity) and clonal *KRAS*$^{G12C}$ mutation (Fig. 1B; Supplementary Figs. S2A–S2E and S3A and S3B). Single-cell sequencing of the C106-resistant subline indicated that the *NRAS*$^{G12D}$ mutation occurred in the same cells bearing the *KRAS*$^{G12C}$ alteration (Fig. 1B), with an acquired gain of the mutant *NRAS* allele occurring in all cells (Fig. 1B). In addition, the subclonal *APC*$^{Q879*}$ nonsense mutation was found to be a late event in tumor evolution (Fig. 1B; Supplementary Figs. S2A–S2E). Copy-number analysis of the resistant RW7213 cells revealed the presence of more than 20 copies of *KRAS*, further validated by fluorescence *in situ* hybridization (FISH; Fig. 1C; Supplementary Fig. S3A and S3B). In parallel, a KRAS$^{G12C}$ mutant colorectal cancer patient-derived xenograft (PDX) model (CLR113) that was initially sensitive to sotorasib and cetuximab combination treatment (6) developed acquired resistance after about 10 months that was associated with amplification of *KRAS*$^{G12C}$ [variant allelic frequency (VAF) 1.00, cancer cell fraction (CCF) 100%], *BRAF*$^{K601E}$ (VAF 0.03, CCF 13%), and *RAF1*$^{S259F}$ (VAF 0.03, CCF 10%) acquired alterations (Fig. 1D and 1E; Supplementary Fig. S4). These data indicate that multiple resistance mechanisms can contribute to the survival of KRAS$^{G12C}$ mutant cells and that *KRAS*$^{G12C}$ amplification may be a recurrent alteration at resistance.

To evaluate resistance mechanisms to KRAS$^{G12C}$ inhibitor and anti-EGFR antibody in patients, we collected circulating free DNA (cfDNA) from 12 patients with colorectal cancer treated with combination treatment [adagrasib plus cetuximab ($n$ = 8) or sotorasib plus panitumumab ($n$ = 4)], who initially experienced tumor regression and then developed either radiographic (RECIST) or clinical progression (Fig. 1F). Patient characteristics and response information are summarized in Supplementary Table S1, and baseline tumor tissue sequencing results are shown in Supplementary Fig. S5. Emergent alterations identified at resistance (Fig. 1G; Supplementary Table S2) included *KRAS*$^{G12C}$ amplification, *KRAS* mutations (G12A/D/F/LR/S/V, H95L/Q/R, and Y96D/H/N), *NRAS* mutations (Q61K/R), downstream ERK pathway alterations (*BRAF* mutations/fusions, *MEK1* mutations), receptor tyrosine kinase (RTK) activation (*MET* amplification/fusion, *RET* fusion, *EGFR* mutations), and *MYC* amplification. Similar to what was previously reported for resistance to KRAS$^{G12C}$ inhibitor monotherapy and in accordance with our preclinical models treated with sotorasib–cetuximab combination, multiple resistance-associated alterations were identified in individual patients, with the majority predicted to prevent inhibition of ERK signaling by drug (12).

### Resistance Dynamics in ctDNA of Colorectal Cancer Patients on KRAS$^{G12C}$–EGFR Inhibition

Similar to resistance alterations to KRAS$^{G12C}$ inhibitor monotherapy (10, 11), all acquired alterations were identified at low VAF, at one tenth or one hundredth of the frequency of alterations identified at baseline. To better understand clonal dynamics of resistance to combination treatment in colorectal cancer, ctDNA was serially collected during treatment and sequenced about every 6 weeks in 4 patients (Fig. 2A–C; Supplementary Table S3). Longitudinal analysis confirmed the emergence of multiple resistance alterations. Resistant alterations often emerged many weeks before the development of clinical resistance and remained at a low frequency, largely <1% VAF, whereas the baseline alterations and tumor marker (CEA) rose higher during treatment. In multiple

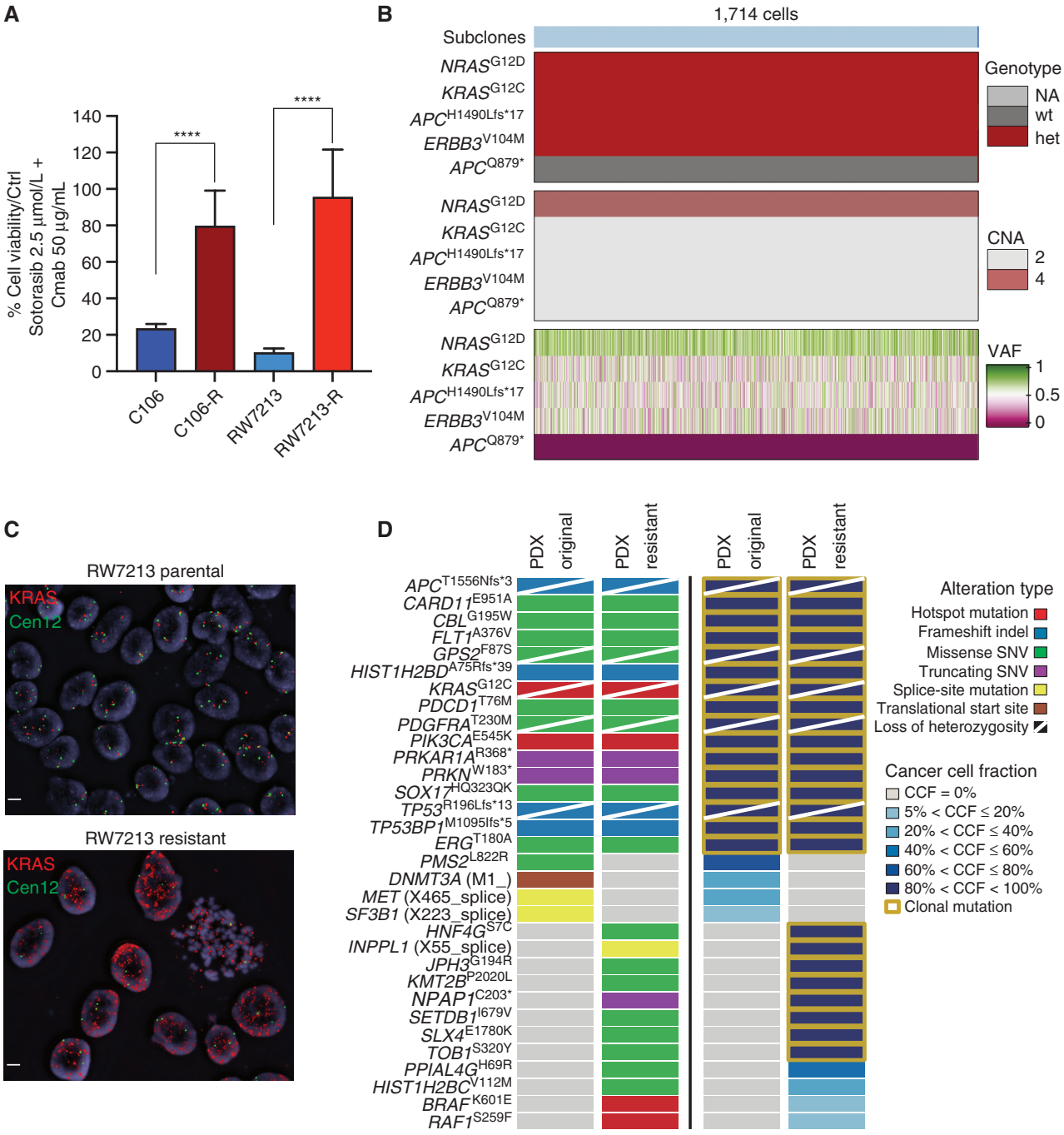


**Figure 1.** Mechanisms of resistance to combined KRAS$^{G12C}$ and EGFR inhibition in colorectal cancer. **A,** Graph showing cell viability of parental and resistant (-R) C106 and RW7213 cells. Statistical analyses and *P* values represent Mann–Whitney test (*t* test); ****, $P \leq 0.0001$. Cmab, cetuximab. **B,** Heat map of *KRAS*$^{G12C}$ and *NRAS*$^{G12D}$ alleles detected by single-cell sequencing of C106 resistant subline. CNA, copy-number alteration; VAF, variant allelic frequency; het, heterozygous mutant; NA, not applicable; wt, wild-type. **C,** FISH staining for the *KRAS* gene in RW7213 parental cells and resistant subline. Manual review of parental RW7213 cells indicated no amplification [mean *KRAS* (red)/Cen12 (green) ratio of 1.1; 50 cells counted] in approximately 90% of the hybridized area and approximately 10% hybridized area with increased *KRAS* copies (mean red/green ratio of 3.5; 50 cells counted). Mean red/green ratio in the resistant subline, based on manual counting of 20 cells, was 6.4 with >20 *KRAS* (red) signals in all cells. Scale bars, 5 µm. **D,** Nonsynonymous somatic mutations identified by MSK-IMPACT in the CLR-113 original and resistant PDXs. Mutation types (left) and CCF of mutations identified (right) are color coded according to the legend. SNV, single-nucleotide variant. (*continued on next page*)

patients, once resistance alterations were first detected, each successive time point identified new resistance alterations with only modest changes in the VAF of the preexisting resistant alterations (Fig. 2A–C; Supplementary Table S3). We did not observe a clonal sweep with the emergence of a dominant resistance alteration in any patient. In several patients, the VAF of the putative resistance alterations actually decreased and became undetectable despite continued treatment.

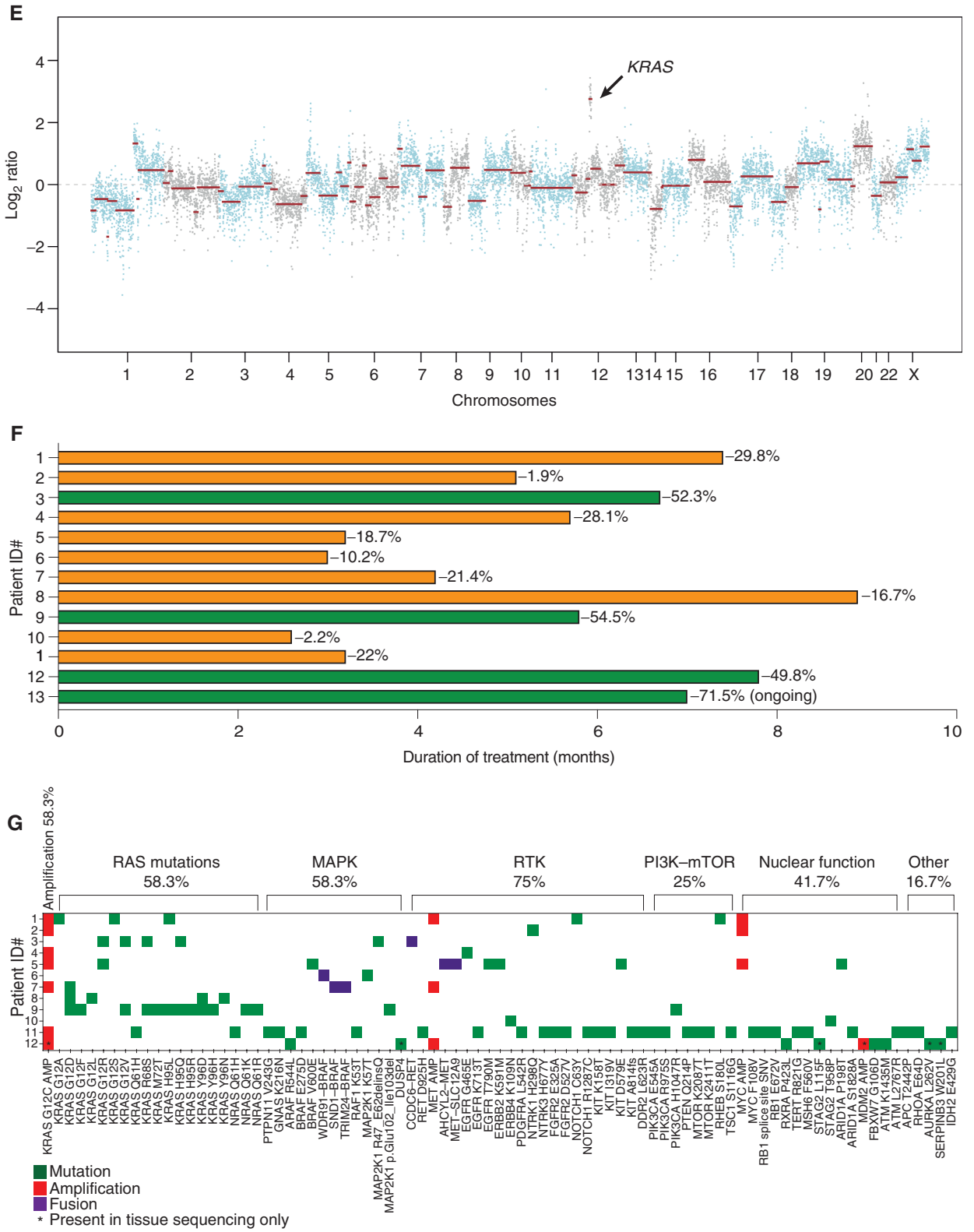


**Figure 1.** ***(Continued)*** **E,** CNAs of the CLR-113 original and resistant PDXs (top). Copy-number $\log_2$ ratios are shown on the *y*-axis according to the chromosomes on the *x*-axis. The arrow shows *KRAS* amplification. **F,** Plot showing duration of response to $KRAS^{G12C}$ inhibitor (adagrasib/sotorasib) plus EGFR inhibitor (cetuximab/panitumumab) by patient ID number. Best response by RECIST is noted at the end of each bar, and partial responses are shaded green and stable disease shaded orange. **G,** Oncoprint of emergent alterations detected in ctDNA of patients with colorectal cancer at the time of radiographic or clinical progression through combined $KRAS^{G12C}$ and EGFR inhibition. Patient 12 had both ctDNA and tumor tissue analyzed at progression, and emergent alterations identified only in tissue are marked with an asterisk. AMP, amplification.

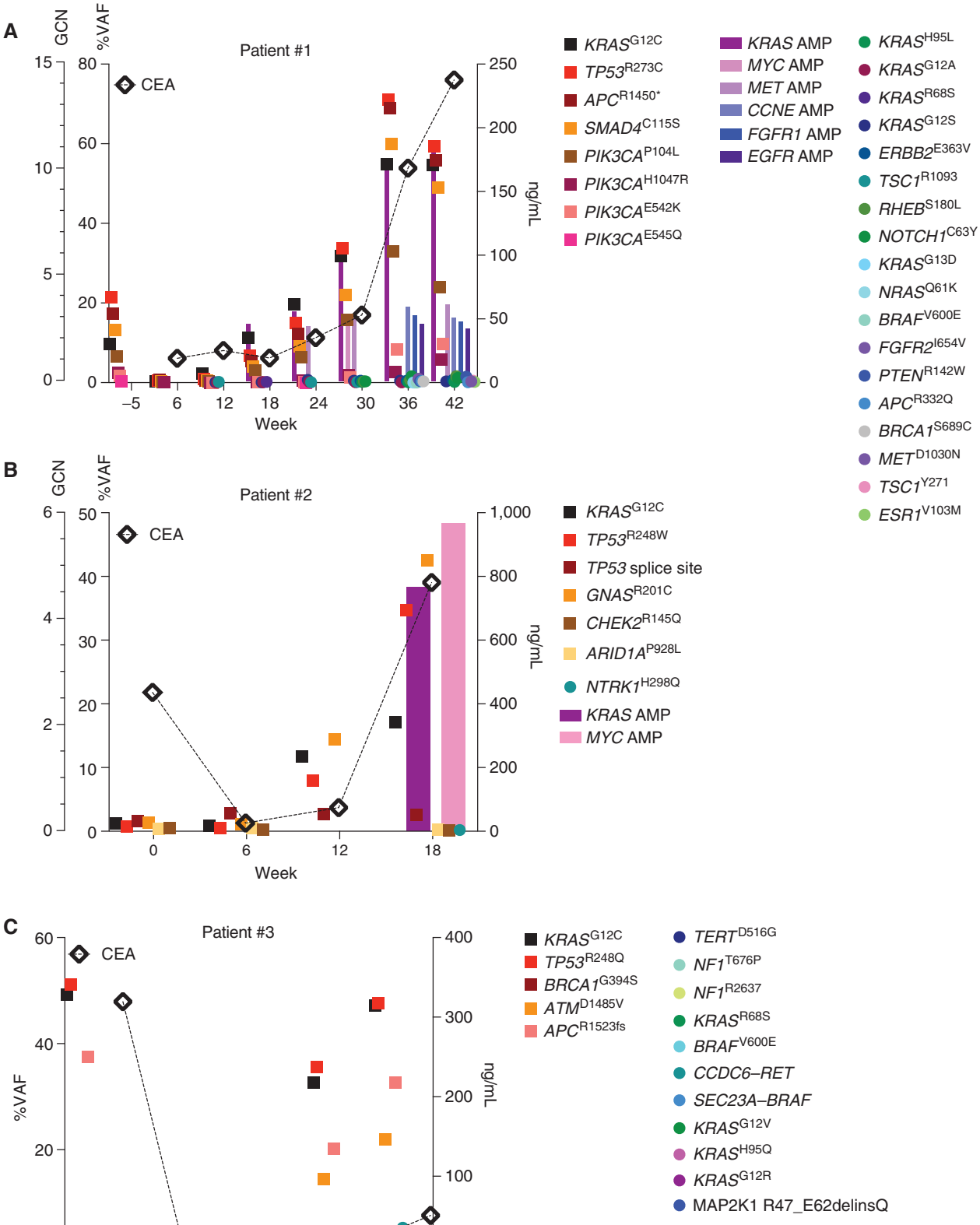


**Figure 2.** Longitudinal analysis of ctDNA in colorectal cancer patients on KRAS$^{G12C}$–EGFR inhibition. **A–C,** Patients with colorectal cancer treated with combined KRAS$^{G12C}$ and EGFR inhibitors: Circles indicate emergent alterations on treatment; bars indicate emergent copy-number changes; and tumor biomarker (CEA) is indicated with a diamond. In all graphs, *KRAS*$^{G12C}$ is marked with solid black square and *TP53* alterations are marked with a red square to track these truncal alterations. AMP, amplification; GCN, gene copy number.

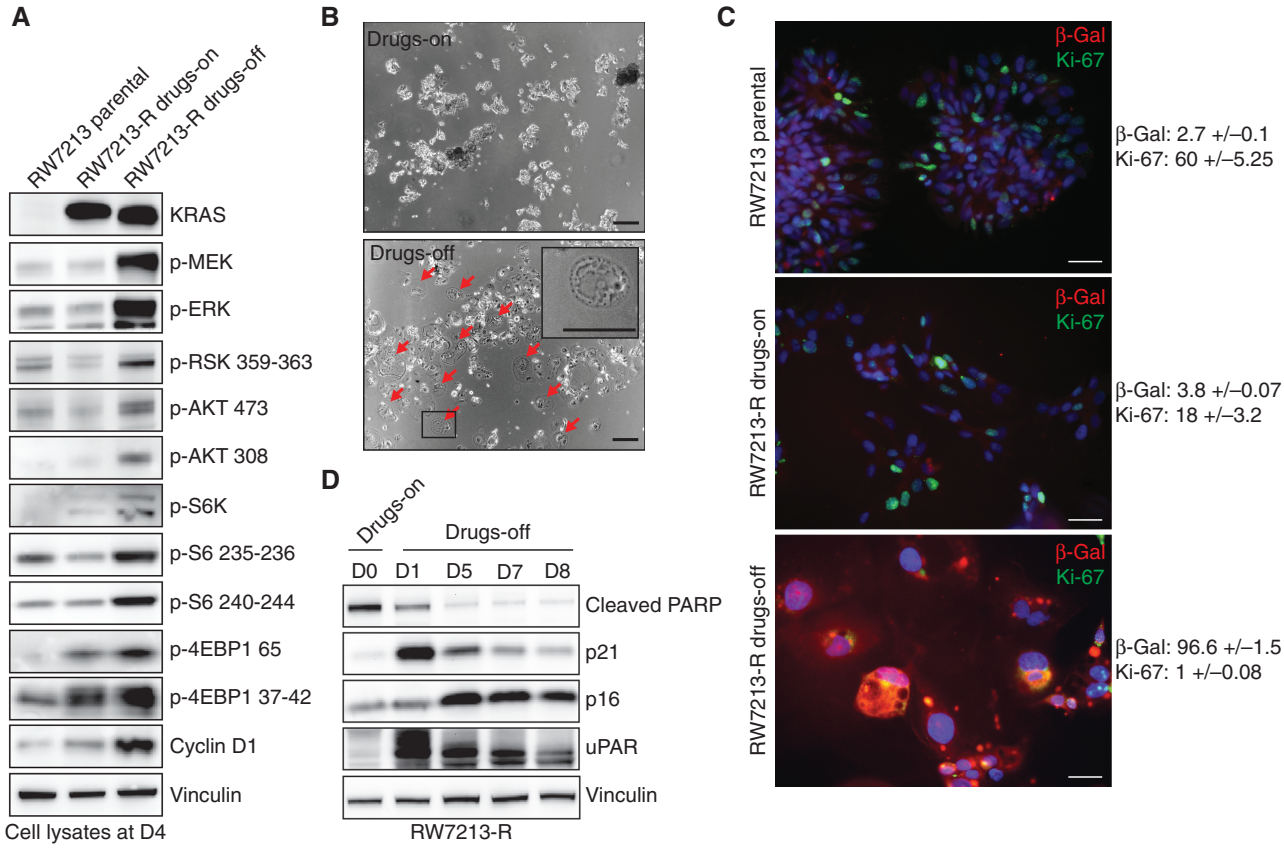


**Figure 3.** Drug withdrawal drives the senescent phenotype in a resistant colorectal cancer cell line with acquired *KRAS*$^{G12C}$ amplification. **A,** Western blot analyses of the effects on MAPK and mTOR pathway regulation in RW7213 parental cells and in RW7213 resistant cells (RW7213-R) with and without cetuximab–sotorasib combination; vinculin is included as a loading control. **B,** Microscopy images of RW7213-R with and without cetuximab–sotorasib combination: 10× magnification; scale bars, 100 μm. In the bottom left corner, the black square represents the area magnified in the upper-right corner inset. The red arrows indicate senescent cells. **C,** Ki-67 and β-galactosidase (β-Gal) staining by immunofluorescence (time point 4 days): 10× magnification; scale bars, 100 μm. Quantification represents the percentage of β-Gal– and Ki-67–positive cells per total number of cells; ± symbol indicates variation between pictures. Ten independent pictures have been quantified per condition. **D,** Western blot analyses of p16, p21, cleaved PARP, and uPAR expression upon drug withdrawal; vinculin is included as a loading control. (*continued on following page*)

These included alterations expected to cause resistance to a KRAS$^{G12C}$ inhibitor, such as the *KRAS*$^{G13D}$, *NRAS*$^{Q61K}$, and *BRAF*$^{V600E}$ mutations detected in patient 1 (Fig. 2A) and the *BRAF*$^{V600E}$ mutation and *BRAF* fusion in patient 3 (Fig. 2C). These data together suggest that resistant subclones do not grow effectively and are unable to grow out to dominate the population. Indeed, among the many low-frequency resistance alterations detected in patients, the only putative resistance genetic event that increased steadily in step with tumor marker response was amplification of the *KRAS*$^{G12C}$ variant. Clinical resistance to KRAS$^{G12C}$ and EGFR inhibition is thus characterized by the accumulation and loss of many low-frequency resistance alterations, whereas *KRAS*$^{G12C}$ amplification drives a higher portion of the resistance phenotype.

## Effect of Drug Withdrawal on *KRAS*$^{G12C}$-Amplified Resistant Cells

Intrigued by the correlation of *KRAS*$^{G12C}$ amplification with clinical resistance, we used the RW7213 resistant cells harboring high-grade *KRAS*$^{G12C}$ amplification to investigate the characteristics of this resistance mechanism. The resistant cells grow as colonies in a medium containing cetuximab and sotorasib, maintaining the same morphology of the parental RW7213 cell line. We then grew these cells in the absence of drugs to mimic the effect of stopping treatment at clinical progression. We found that *KRAS* amplification was maintained in the resistant RW7213 cells with short-term drug withdrawal, and analysis of RAS downstream effector signaling in RW7213 parental, resistant, and resistant cells off drugs showed instead further increase of MAPK and Pi3K–mTOR pathway activation upon drug withdrawal in the resistant cells compared with the resistant cells on drugs and parental RW7213 cells (Fig. 3A).

Together with these effects on signaling, we also observed that 24 to 48 hours after drug withdrawal, RW7213 *KRAS*$^{G12C}$-amplified cells acquired a large and flat morphology, and this phenotype was maintained over time (Fig. 3B). This feature is reminiscent of cellular senescence, a program that can be triggered by excessive oncogenic signaling (14). RW7213 resistant cells in which the drug was withdrawn showed an increase in β-galactosidase activity and decrease in cellular proliferation, as measured by Ki-67 staining, both consistent with a senescent phenotype (Fig. 3C). Senescent cells acquire a new metabolic state, are protected from apoptosis, and

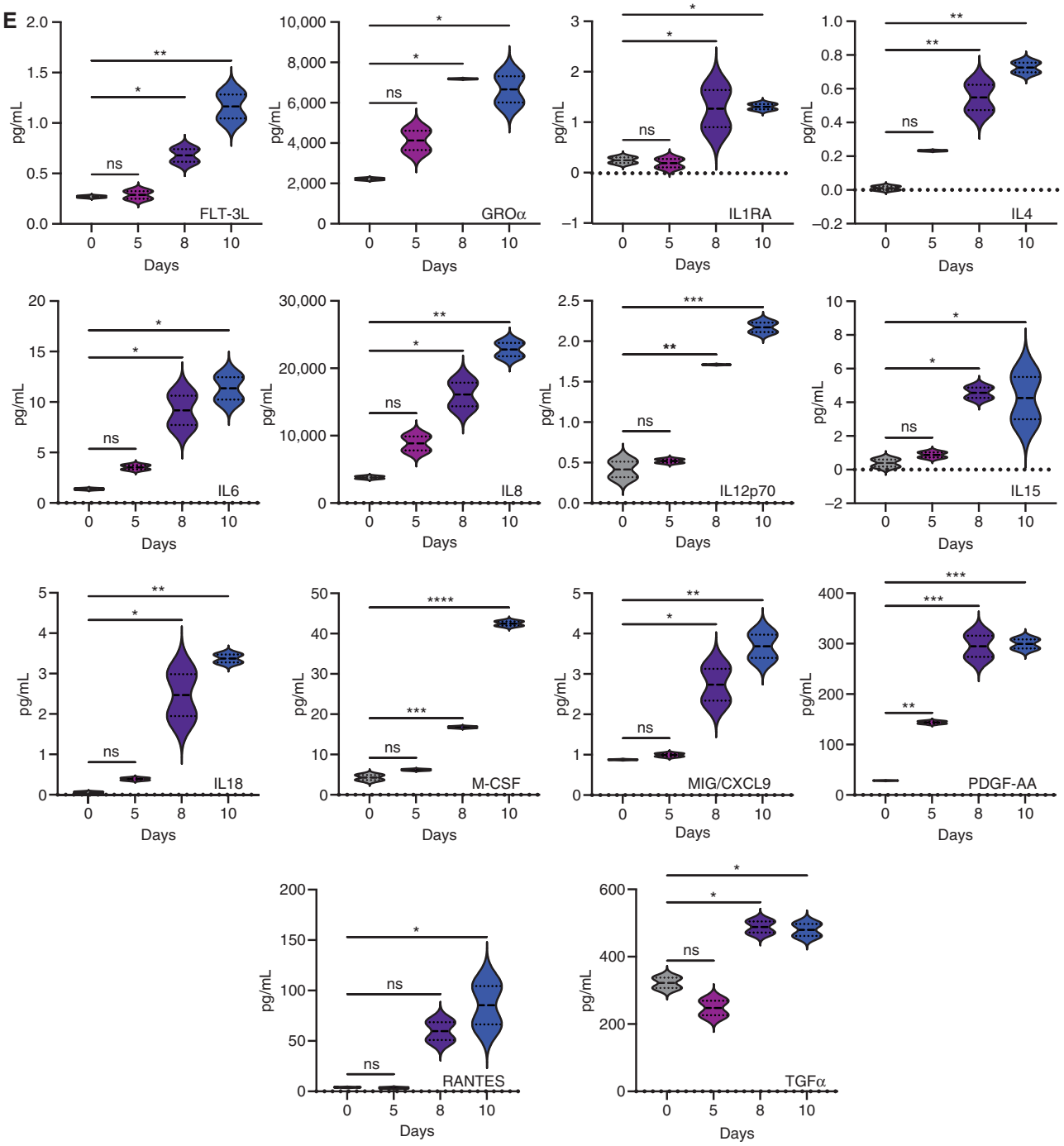


**Figure 3.** ***(Continued)*** **E,** SASP cytokine array time-course experiment. Data shown represent duplicates. Statistical analyses and *P* values represent two-way ANOVA with Dunnett multiple comparisons test. ns (not significant) = $P > 0.05$; *, $P \leq 0.05$; **, $P \leq 0.01$; ***, $P \leq 0.001$; ****, $P \leq 0.0001$. (*continued on next page*)

activate a secretory program known as the senescence-associated secretory phenotype (SASP; refs. 15–17). In line with a senescent phenotype, RW7213 resistant cells taken off the drug combination downregulated apoptosis markers; increased expression of cyclin-dependent kinase inhibitors and uPAR, a marker of senescence (18); and accumulated cytokines indicative of SASP (Fig. 3D and E). By contrast, C106 resistant cells harboring *KRAS*$^{G12C}$ and *NRAS*$^{G12D}$ mutations did not exhibit the senescence phenotype or markers (Supplementary Fig. S6A and S6B), suggesting that this effect is specific for *KRAS*$^{G12C}$ amplification. These data suggest that high levels of KRAS signaling, which are needed to drive resistance to the drugs, trigger oncogene-induced senescence upon drug withdrawal.

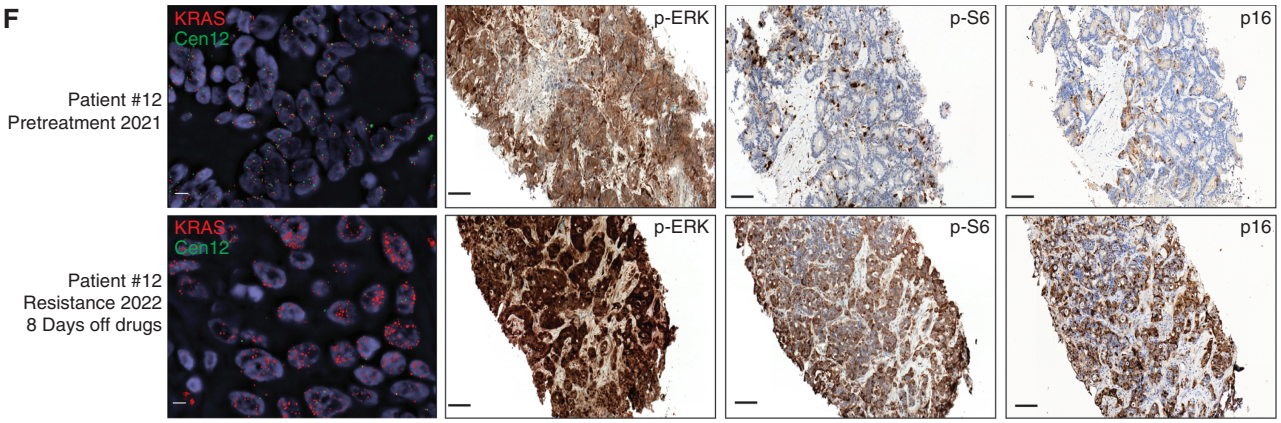


**Figure 3.** ***(Continued)*** **F,** FISH staining for *KRAS* (scale bar, 5 μm) and IHC for p-ERK, p-S6 (S235), and p16 in tissue samples collected from patient 12, consisting of pretreatment liver metastasis biopsy (pretreatment 2021) and progression liver metastasis biopsy collected 8 days after stopping $KRAS^{G12C}$ and EGFR inhibitors (resistance 2022). Mean *KRAS* (red)/Cen12 (green) ratio, based on manual counting of 50 cells from each time point, was 1.8 for the pretreatment specimen and 13.2 for the resistance specimen. p-ERK staining was 2+ involving >90% of cells pretreatment and 3+ involving >90% of cells at progression; p-S6 staining was absent pretreatment and 2+ involving 70% of cells at progression; and p16 staining was 2+ involving 5% of cells pretreatment and 2+ involving 65% of cells at progression. Magnification of all IHC slides is 20×; scale bars, 100 μm.

To check for similar changes in the clinical setting, we evaluated activation of the MAPK and mTOR pathways in tissue samples from a patient who developed $KRAS^{G12C}$ amplification at resistance (Fig. 1E). Several patients with colorectal cancer had identifiable $KRAS^{G12C}$ amplification at resistance, and patient 12 underwent biopsy of a liver metastasis immediately before starting $KRAS^{G12C}$ and EGFR inhibitors (pretreatment 2021) and again at progression where tissue was collected 8 days after the stop of $KRAS^{G12C}$ and EGFR inhibitor drug therapy and before the start of any new therapy (resistance 2022; Fig. 3F). Sequencing and FISH showed acquired high-level *KRAS* amplification at progression (Fig. 3F; Supplementary Fig. S6C). Phosphorylated ERK levels were high pretreatment (2+ staining involving >90% of cells) and further increased at progression (3+ staining involving >90% of cells). Phosphorylated ribosomal protein S6 (S235) levels were low prior to treatment (absent staining) and elevated (2+ staining involving 70% of cells) in the progression sample collected after 8 days of drug withdrawal (Fig. 3F). These data demonstrate in a patient progressing with $KRAS^{G12C}$ amplification that, after drug stop, tumor tissue has elevated MAPK and mTOR pathway signaling. We further checked changes in p16 levels, which commonly associates with senescence (19), in these clinical samples as a marker for senescence and found rare staining pretreatment (2+ staining, involving 5% of cells) and increased p16 expression at progression (2+ staining, involving 65% of cells; Fig. 3F). These data provide the support that, in patients, tumors with acquired *KRAS* amplification may also undergo senescence changes upon drug withdrawal.

## Exploiting the New Steady State after Drug Withdrawal to Overcome Resistance

Given the dramatic effect of drug withdrawal, we wondered if $KRAS^{G12C}$ amplification produces a selective disadvantage upon drug withdrawal in the clinical setting and monitored ctDNA in two of the patients with colorectal cancer with acquired $KRAS^{G12C}$ amplification at resistance. We followed the ctDNA of patients 1 and 5, who both harbored $KRAS^{G12C}$ mutant colorectal cancer that had developed multiple resistance alterations, including $KRAS^{G12C}$ amplification (Figs. 1E and 2A). Comparison of ctDNA from before and about 4 weeks after drug withdrawal in each of these patients showed a 2-fold reduction of the signal from *KRAS* amplification. By contrast, the relative frequency of the other preexisting alterations and emergent mutations remained mostly unchanged (Fig. 4A and B; Supplementary Table S3). Together, these data suggest that $KRAS^{G12C}$ amplification is a mechanism of secondary resistance that shows fitness only in the presence of the selective pressure mediated by drug treatment.

Hence, we used the RW7213 resistant cells to investigate the effects of MAPK signaling suppression after a period of drug removal. After stopping cetuximab–sotorasib combination treatments, we rechallenged the cells with either the same combination (Fig. 4C) or with the MEK inhibitor trametinib (Fig. 4D) as a function of time. While drug treatment was able to significantly decrease MAPK signaling, the cells maintained higher levels of p-S6K and p-S6 that were not suppressed by drug treatment, suggesting a new steady state after drug withdrawal with higher mTOR pathway signaling. mTOR signaling activation has been associated with senescence, as it regulates several senescence-associated phenotypes (15). p-ERK was inhibited best after the shortest time off drug (2 days), and this time point was associated with a lower induction of p-S6 levels. However, rechallenge at longer time points could not suppress mTOR signaling or restore apoptotic potential (cleaved PARP).

These data suggest that periods of drug withdrawal and retreatment will be unable to reestablish drug sensitivity and cell death. However, we hypothesized that the senescent state and associated activation of mTOR-dependent signaling in these cells may provide a therapeutic vulnerability. Indeed, the mTOR inhibitor AZD8055, which has been previously proposed as a senolytic agent (20), was able to inhibit S6K and S6 phosphorylation selectively in RW7213 resistant cells in which drug was removed (Fig. 4E). Proliferation assays show that RW7213 cells off drug are more sensitive to AZD8055 than cells maintained

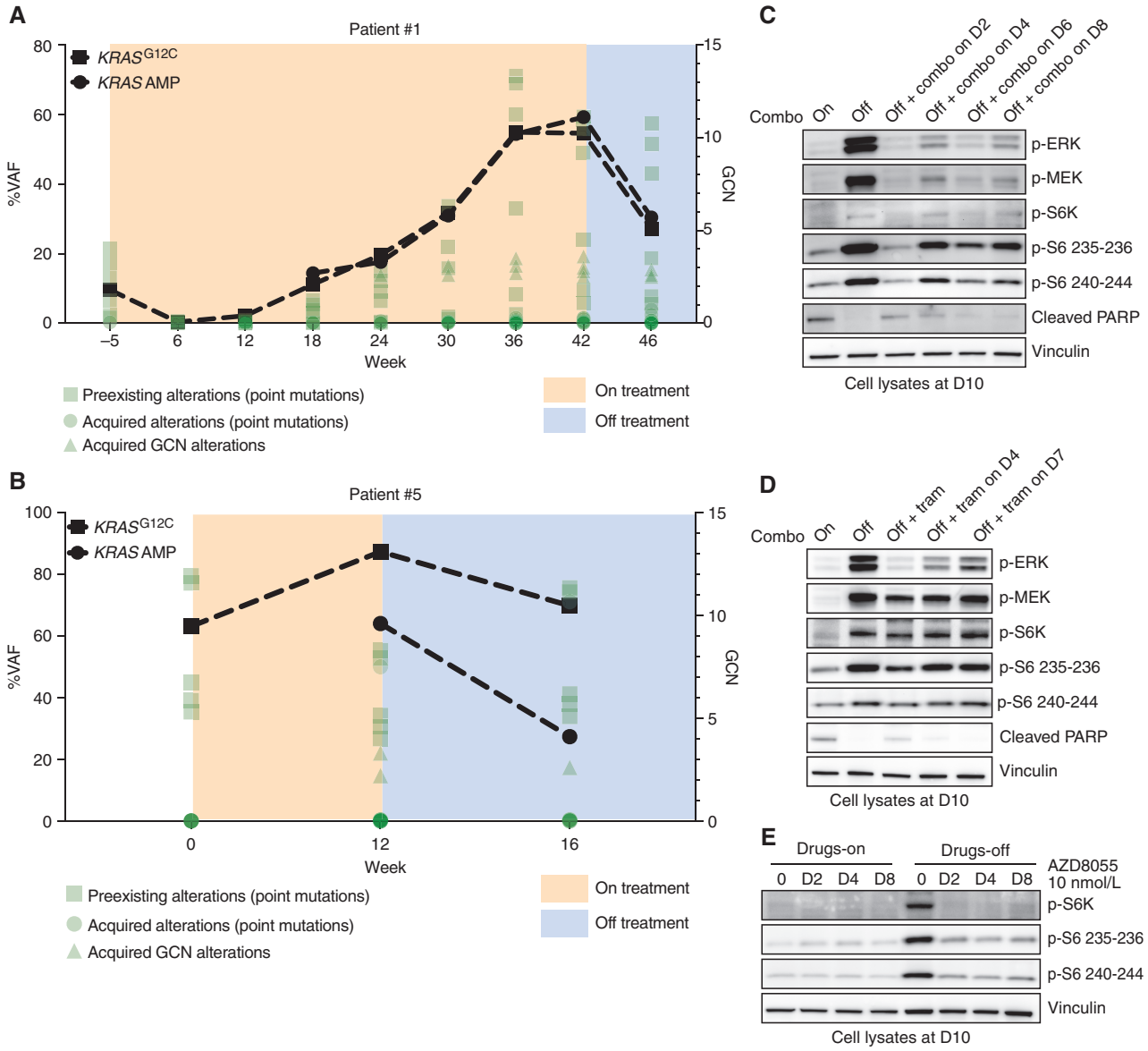


**Figure 4.** Effect of treatment withdrawal in resistant colorectal cancers with amplified *KRAS*$^{G12C}$. **A** and **B,** Longitudinal analysis of ctDNA in colorectal cancer patients who held KRAS and EGFR inhibition for approximately 4 weeks after progression. *KRAS*$^{G12C}$ ctDNA VAFs are marked with squares, and *KRAS* plasma copy numbers are marked with circles. All the other variants are reported in green. AMP, amplification; GCN, gene copy number. **C,** Western blot analyses of p-ERK, p-MEK, p-S6K, p-S6, and cleaved PARP expression upon drug withdrawal and rechallenge with 50 μg/mL cetuximab and 3 μmol/L sotorasib combination; vinculin is included as a loading control. **D,** Western blot analyses of p-ERK, p-MEK, p-S6K, p-S6, and cleaved PARP expression upon drug withdrawal and rechallenge with 10 nmol/L trametinib (tram); vinculin is included as a loading control. **E,** Western blot analyses of p-S6K and p-S6 upon drug withdrawal or in drug-containing medium after treatment with 10 nmol/L AZD8055; vinculin is included as a loading control. (*continued on next page*)

with continuous drug exposure (Fig. 4F). To support the specificity of mTOR inhibition, we used another senolytic drug, the BCL2 inhibitor navitoclax (21), and this compound failed to block cell proliferation in the RW7213 resistant cells after drug withdrawal or with continuous drug exposure (Fig. 4G).

Altogether, these data suggest that there may be enhanced activity and selectivity of mTOR blockade in resistant KRAS$^{G12C}$ cancers with *KRAS*$^{G12C}$ amplification following drug withdrawal and nominates further exploration of a one–two punch approach of drug withdrawal and senolytic therapy as a potential strategy to overcome acquired resistance to EGFR–KRAS$^{G12C}$ combination in those tumors that acquired *KRAS*$^{G12C}$ amplification (Fig. 4H).

## DISCUSSION

Here, we report the genetic mechanisms of secondary resistance to concomitant EGFR and KRAS$^{G12C}$ blockade in KRAS$^{G12C}$ mutant colorectal cancer. In agreement with previous studies, our patients show subclonal heterogeneity and acquired mutations at low variant allele frequencies. This may be due in part to the evaluation of ctDNA, as this method

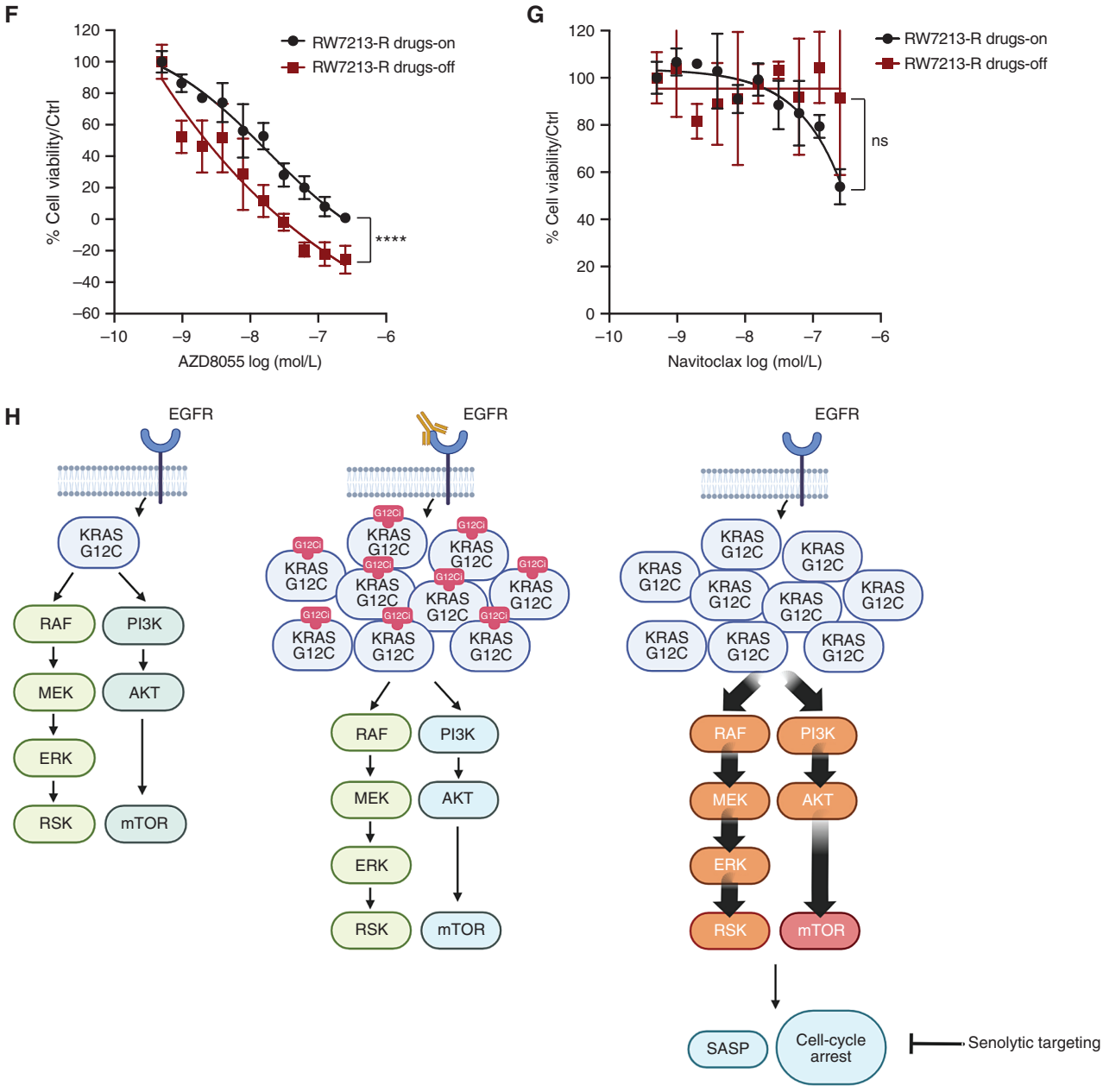


**Figure 4.** ***(Continued)*** **F,** Short-term proliferation assay of RW7213 resistant cells (RW7213-R) in medium containing cetuximab–sotorasib (black) and in senescent conditions (dark red). Cells were seeded in the absence or presence of drugs for 4 days and then treated for 96 hours with increasing concentrations of AZD8055, and then ATP content was measured using CellTiter-Glo. Data represent the average and standard deviation of 3 biological replicates. ns (not significant) = $P > 0.05$; ****, $P \leq 0.0001$. **G,** Short-term proliferation assay of RW7213-R in medium containing cetuximab–sotorasib (black) and in senescent conditions (dark red). Cells were seeded in the absence or presence of drugs for 4 days and then treated for 96 hours with increasing concentration of navitoclax, and then ATP content was measured using CellTiter-Glo. Data represent the average and standard deviation of 3 biological replicates. **H,** Proposed model: $KRAS^{G12C}$ mutant signaling is maintained at a similar level in parental cells and in resistant cells in the presence of concomitant EGFR and $KRAS^{G12C}$ blockade. Upon drug removal, *$KRAS^{G12C}$*-amplified signaling drives oncogene-induced senescence characterized by elevated mTOR activity, creating a new steady state that may be targeted by senolytic treatments.

exposes tumor heterogeneity more than single biopsy specimens (22). Sequencing data from our study and others (10–12) might suggest that a small fraction of cells may be sufficient to drive clinical resistance. This concept is in line with recent studies of metastatic behavior in which, for example, single-cell RNA sequencing of small-cell lung cancers identified a rare population of stem-like cells that appears to drive metastatic outcomes in this cancer (23). However, our study highlights that these low frequency alterations appear and disappear during treatment, and this may support an induction of mutagenesis due to drug (24) and also that these lesions can be characterized by low fitness and may not effectively drive resistance.

In contrast to the low frequency resistance mechanisms, we identify *$KRAS^{G12C}$* amplification as a recurrent resistance

mechanism that tracks with tumor markers and response and engages oncogene-induced senescence when the drug is removed. Previous reports showed that *BRAF* amplification upon RAF inhibitor resistance can be modulated by intermittent treatment (25), and we show that amplified *KRAS*$^{G12C}$ recedes in the absence of drug in patients' plasma. Here, we describe the transition to a senescence state in a cell line and patient's tumor and hypothesize that the drop of KRAS$^{G12C}$ in ctDNA is due to the protective effect of senescence from apoptosis and consequently the release of cell-free DNA. We also show in the cell line that the senescent phenotype that has high mTOR pathway activation prevents a strategy of intermittent therapy from overcoming resistance, and that in clinical samples from a patient with acquired *KRAS* amplification, mTOR pathway signaling is induced after drug release and correlates with p16 induction as a marker of senescence. These results provide a possible mechanistic explanation for the worse outcomes seen with intermittent RAF inhibition for melanoma treatment in the clinic (26).

Oncogene overexpression *in vitro* is challenging, as cells select against this hyperactivation over time, and we were unable to generate KRAS$^{G12C}$-overexpressing cell lines. This suggests that *KRAS*$^{G12C}$-amplified cells need the adaptation underlying long-term drug exposure and acquired resistance to therapy and raises questions about what mechanisms regulate this adaptation and how can we target them.

Our data, however, nominate a new potential approach to overcome acquired resistance by exploiting vulnerabilities due to the senescence program during periods of drug withdrawal to target resistant cells more broadly. In this work, we took advantage of the new dependency on mTOR signaling that develops when cells enter the senescent state because of excessive oncogenic RAS signaling. Activation of mTOR-dependent signaling is required for maintenance of cellular senescence (15, 27), and drug withdrawal can be combined with senolytic approaches (28) to facilitate tumor clearance, as shown by us and others, by inhibition of mTOR signaling (20). Additional mechanistic insights into mTOR activation and longer-term drug-off kinetics will be important to examine further in future studies. Other potential senolytic approaches can be based on exploiting SASP chemokines that can recruit immune cells, suggesting the potential to target resistant cancer cells with immune-checkpoint inhibitors (29–32). Moreover, senescence-driven expression of uPAR could also become a target for chimeric antigen receptor T-cell therapy (33). Further studies will provide important insights on how to effectively target KRAS$^{G12C}$ mutant cancers that developed secondary resistance to KRAS$^{G12C}$ inhibitors as single agents and in combination.

## METHODS

### Cell Lines and Compounds

The RW7213 cell line was cultured in RPMI (Lonza). The C106 cell line was cultured in Iscove's modified medium (Lonza). Each media was supplemented with 10% FBS, 2 mmol/L L-glutamine, 100 U/mL penicillin, and 100 mg/mL streptomycin. Resistant derivatives were grown in media containing cetuximab (50 μg/mL) and sotorasib (3 μmol/L). C106 cells were purchased from ECACC, and RW7213 was provided by Dr. Diego Arando (Group of Molecular Oncology, Nanomedicine Research Program, Molecular Biology and Biochemistry Research Center, CIBBIM Nanomedicine, Vall d'Hebron Hospital Research).

All the cell lines were determined to be *Mycoplasma* free using the Venor GeM Classic kit (Minerva Biolabs, last test July 2022) and tested by short tandem repeat profiling at 10 different loci.

Sotorasib and trametinib were purchased from SelleckChem. Cetuximab was purchased from the Pharmacy at Memorial Sloan Kettering Cancer Center (MSKCC).

### Cell Viability Assay

For dose–response proliferation assays, 4,000 cells were seeded in 96-well culture plates in complete medium. After 24 hours, the indicated concentrations of sotorasib and cetuximab were added to cell. After 72 hours, cell viability was determined by measuring ATP content using CellTiter-Glo Luminescent Cell Viability assay (Promega). DMSO-only treated cells were used as control. Assays were performed with 3 replicates and were each repeated three times. For senolytic proliferation assays with RW7213 resistant cells, 2,000 cells were seeded in 96-well culture plates in a medium containing the combination of 50 μg/mL cetuximab and 3 μmol/L sotorasib or medium only to induce senescence. After 96 hours, serial dilutions of AZD8055 or navitoclax were added to cells, and cell viability was determined at baseline by measuring ATP content using CellTiter-Glo Luminescent Cell Viability assay (Promega). After 96 hours, cell viability was determined again by measuring ATP content using CellTiter-Glo Luminescent Cell Viability assay (Promega). DMSO-only treated cells were used as control, and all the values were normalized on baseline measurements. In all the experiments, plates were incubated at 37°C in 5% $CO_2$.

### Antibodies and Western Blotting

After seeding and drug treatments, cells were washed with cold PBS and lysed in RIPA buffer (Pierce, #89901) plus phosphatase and protease inhibitors (Thermo Scientific, #1861277, #1861278). Lysates were cleared by centrifugation at 14,000 rpm at 4°C and quantified using the BCA method (Pierce, #23224).

Samples were prepared using LDS + Reducing agent Novex buffers (Invitrogen, #NP0008, #NP0009). Ten to 20 μg of lysates were loaded and run on NuPageTM 4% to 12% Bis-Tris gels (Thermo Fisher, #NP0321BOX) followed by transfer to nitrocellulose membranes (Bio-Rad, #1620233). Membranes were incubated overnight with the indicated antibodies, washed, and incubated again for 45 minutes with anti-rabbit or anti-mouse secondary antibodies. Detection was performed using Immobilion Western (Millipore; #WBKLS0500).

The following primary antibodies were obtained from Cell Signaling Technology and were used at a concentration of 1:1,000: anti-p16 (#80772), anti-p21 12D1 (#2947), anti-Actin (#4970), anti–p-MEK1/2 S217/221 (#9154), anti–p-p44/42 MAPK T202/204 (#9101), anti–total ERK1/2 (#9102), anti–p-AKT 473 (#4060), anti–p-S6K(#9204), anti–p-S6 235-236 (#4858), anti–p-S6 240–244(#5364), anti-uPAR (#12713), anti–p-RSK (#9944), anti–p-4E-BP1 65 (#9451), anti–p-4E-BP1 37/42 (#2855), and anti-Vinculin (#13901S). Anti–Cyclin D1 antibody was purchased from Thermo Scientific (PA516777) and used at 1:1,000 dilution. Anti-KRAS and anti-NRAS were purchased from Santa Cruz Biotechnology and used at 1:500; anti-p338-CRAF was purchased from Millipore and used at 1:1,000.

### RAS-GTP Pulldown Assay

RAS-GTP pulldown assay was performed according to the manufacturer's protocol (Thermo Scientific; #16117). Briefly, 500 μg of lysates was loaded into columns together with agarose beads and RAS-RBD bait and incubated for 1 hour at 4°C. After the incubation, beads were washed three times and resuspended in LDS + Reducing agent Novex buffers (Invitrogen; #NP0008, #NP0009). A fraction of lysates was used to measure total RAS amount. Pulldown and total lysates were subjected to the Western blotting procedure as described above. The kit provided primary antibody against pan-RAS.

### SASP Cytokine Array

Conditioned media were collected from cells that were cultured in the presence or absence of the drug combination. Aliquots of the media were analyzed with a multiplex immunoassay designed for human samples, "Human Cytokine Array/Chemokine Array 48-Plex HD48" (Eve Technologies). Cytokine concentration was normalized by cell count.

### In Vivo *Studies*

The CLR113 PDX was derived from liver metastasis. Tumor tissue was transplanted orthotopically into NSG mice to establish the PDX (Institutional Review Board protocols 06-107, 14-091). Once a tumor became visible in the first mouse, it was transplanted and expanded to other animals. Tumor tissue was implanted subcutaneously in the flank of 4- to 6-week-old NSG female mice, and treatment of the mice began when the tumor reached approximately 100 $mm^3$ in size. Mice were randomized ($n$ = 5 mice per group) to receive drug treatments or vehicle as control.

Sotorasib (100 mg/kg) and trametinib (3 mg/kg) were given daily by gavage. Cetuximab was administered 50 mg/kg twice a week by intraperitoneal injections.

Studies were performed in compliance with institutional guidelines under an Institutional Animal Care and Use Committee (IACUC)–approved protocol. The animals were immediately euthanized as soon as the tumors reached the IACUC set limitations.

### Patients

All patients were treated on KRAS inhibitor clinical trials approved by the MSKCC Institutional Review Board/Privacy Board [protocols 19-408 (NCT03785249), 20-183 (NCT04185883)]. Collection of patient samples was conducted under appropriate Institutional Review Board/Privacy Board protocols and waivers (protocols 06-107, 12-245, 14-019). Participating patients signed written informed consent for these clinical trials and biospecimen protocols. This study was conducted in accordance with ethical guidelines in the Declaration of Helsinki.

### FISH

FISH analysis was performed on adherent cells. KRAS FISH analysis was performed using a 2-color KRAS/Cen12 probe mix (developed at MSKCC). The probe mix consisted of bacterial artificial chromosome clones containing the full-length *KRAS* gene (clones RP11-29515 and RP11-707F18; labeled with red dUTP), and a centromeric repeat plasmid for chromosome 12 served as the control (clone pa12H8; labeled with green dUTP). Probe labeling, hybridization, washing, and fluorescence detection were performed according to standard procedures. Slides were scanned using a Zeiss Axioplan 2i epifluorescence microscope equipped with a megapixel CCD camera (CV-M4$^+$CL, JAI) controlled by Isis 5.5.9 imaging software (MetaSystems Group Inc.). The entire section was scanned through 63X or 100X to assess signal patterns and select representative regions for imaging. Amplification was defined as >10 copies of each locus.

### Combined β-galactosidase and Immunofluorescence Staining

For immunofluorescent staining, 20,000 cells/well were seeded in a Nunc Lab-Tek II Chamber Slide System (Thermo Fisher, 154526). β-galactosidase staining was performed using ImaGeneRed $C_{12}$RG (I-2906) according to the manufacturer's instruction with a final concentration of 33 mmol/L $C_{12}$RG compound for 2 hours. To stop β-galactosidase activity, PETG was added to the medium. Cells were fixed with 4% PFA for 10 minutes at RT, permeabilized using 0.02% Triton/PBS, and incubated with Ki-67 antibody (Abcam, ab16667) overnight in 0.02% Triton/5% BSA/PBS. A secondary antibody was added the day after, and DAPI was used to stain the nucleus. Slides were mounted using ProLong Gold Antifade Mountant (Thermo Fisher, P10144). Pictures were quantified using Fiji Software, and 10 independent pictures have been quantified per condition.

### DNA Sequencing

***cfDNA Analysis.*** cfDNA analysis was performed using the commercially available, targeted next-generation sequencing assays Guardant360 CDx (Guardant Health; patients 1–5, 11) and ctDx FIRST (Resolution Bioscience; patients 6–10) and the MSK-ACCESS assay (patient 12). Guardant360 CDx is a Clinical Laboratory Improvement Amendments–accredited, New York State Department of Health–approved cfDNA assay with analytic and clinical validation previously reported (34, 35). During this study, the assay included an assessment of 74 to 83 genes (depending on panel version ordered) with coverage of single-nucleotide variants (SNV) and select insertions/deletions, amplifications, and fusions. Resolution Bioscience ctDx FIRST assay includes assessment of 113 genes and detects SNV/indel hotspots, SNV/indel full coding sequences (CDS), amplifications, deletions, gene rearrangements, and gene fusions. The ctDx FIRST assay uses a custom bioinformatics pipeline to call variants associated with genomic targets. The MSK-ACCESS assay is a custom, ultradeep assay that includes key exons and domains of 129 genes and introns of 10 genes harboring recurrent breakpoints. It uses duplex unique molecular identifiers and dual index barcodes to minimize background sequencing errors and sample-to-sample contaminations, and alterations are called against matched normal DNA. The longitudinal ctDNA analysis in this study was performed with the Guardant360 CDx assay.

***Bulk Tissue Sequencing.*** Genomic DNA was extracted from cell lines, frozen xenograft tumors, or formalin-fixed, paraffin-embedded patient tissues obtained from biopsies or resections and sequenced with the MSK-IMPACT next-generation sequencing assay (13). Copy-number alterations (CNA) and loss of heterozygosity were defined using FACETS (36). The CCFs of somatic mutations identified in the cell lines and frozen xenograft tumors were computed using ABSOLUTE (v1.0.6; ref. 37), and a mutation was classified as clonal if its probability of being clonal was >50% or if the lower bound of the 95% confidence interval of its CCF was >90%, as previously described (38). For the construction of phylogenetic trees based on CNAs, major and minor copy numbers computed by FACETS (36) were modeled using transducer-based pairwise comparison functions using MEDICC (39), assuming a diploid state with no CNAs to root the phylogenies.

***Single-Cell DNA Sequencing.*** The C106 resistant cell line was subjected to single-cell sequencing. The cell line was washed with PBS and quantified by combining 5 μL of cell suspension with an equal amount of Trypan Blue, loaded on chamber slides, and counted with the Countess automated cell counter (Invitrogen). A total of 250,000 cells were used for the barcoding run. In brief, cells were encapsulated with lysis buffer (100 mmol/L Tris at pH 8.0, 0.5% IGEPAL, proteinase K 1.0 mg/mL) in a Tapestri platform (Mission Bio) and further lysed on the thermal cycler with the following conditions: 60 minutes at 50°C and 10 minutes at 80°C. The DNA from the encapsulated cell lysate was then primed and barcoded using a custom panel (Mission Bio), which targets hotspot variants of 54 oncogenes and tumor suppressor genes, for a total of 317 amplicons. After exposure to UV light, droplet PCR reactions were thermocycled with the following conditions: 6 minutes at 98°C, 10 cycles of 30 seconds at 95°C, 10 seconds at 72°C, 9 minutes at 61°C, and 20 seconds at 72°C; 10 cycles of 30 seconds at 95°C, 10 seconds at 72°C, 9 minutes at 48°C, and 20 seconds at 72°C; and a final step of 2 minutes at 72°C. PCR products were digested at 37°C for 60 minutes and posteriorly purified using 0.63× of SPRI beads (Beckman Coulter). Sample indices and Illumina adapter sequences

were then added via a 9-cycle PCR reaction, and a second 0.63× SPRI purification was then performed on the completed PCR reactions. Libraries were analyzed on a DNA 1000 assay chip with a Bioanalyzer (Agilent Technologies) and sequenced on a NextSeq 550 instrument (Illumina, Inc.; 150-bp, paired-end reads). Sequence data were analyzed using the proprietary software provided by Mission Bio (40). In brief, sequence reads were trimmed for adapter sequences using Cutadapt (41) and mapped to the hg19 human genome using the Burrows–Wheeler Aligner (BWA; ref. 42) after extracting barcode information. Following mapping, on-target sequences were selected using the standard bioinformatics tool (SAMtools; ref. 43), and barcode sequences were error-corrected based on a white list of known sequences (40). The number of cells was determined from barcodes based on the number of reads assigned to each barcode and amplicon read completeness. HaplotypeCaller (GATK v4.2.1.0; refs. 44, 45) was used to genotype the mutations present in all single cells with a joint-calling approach. The mutations identified in each cell were further intersected with MuTect2 (GATK v4.2.1.0; refs. 44, 46) to obtain high-confidence mutations. Genotyping calls were further examined and corrected according to variant allele frequency. Potential doublets or multiplets characterized by the existence of 2 or more cells that are captured within a droplet and linked to a single barcode were identified using DoubletD (47) and further excluded from the analysis. For genotype clustering analysis of the five known variants (*KRAS*$^{G12C}$, *NRAS*$^{G12D}$, *APC*$^{H1490Lfs*17}$, *ERBB3*$^{V104M}$, and *APC*$^{Q879*}$), cells were included when these five variants met the criteria of read depth (≥10) and genotyping quality (≥60; ref. 48). In addition, subclones with a higher allele dropout (ADO) rate compared with the overall ADO rate of all cells were further excluded (49). For clonal architectures, fishplot was created using the fishplot package (50).

To estimate allele-specific CNAs, we used a pool of single, nonneoplastic, diploid cells identified in endometrioid endometrial tumors (51). Read counts of amplicons for C106 resistant and nonneoplastic cells were obtained from MissionBio's pipeline and further used for allele-specific copy-number estimation. Amplicon read counts for cells with no coverage were imputed according to neighboring cells using MAGIC (52). Imputed read counts were normalized to total library size for each cell. Amplicon copy-number ratio was calculated by dividing C106-R read counts with the median of nonneoplastic counts. Because C106-R cells were considered to be diploid in the matched bulk sequencing data, the amplicon copy-number ratio was further transformed into noninteger copy number by multiplying by 2. Finally, the gene integer copy number was obtained by taking the median value of the amplicon copy number for each gene and by taking the nearest integer value.

### IHC

Samples were loaded into Leica Bond RX and pretreated with EDTA-based epitope retrieval ER2 solution (Leica, AR9640) for 20 minutes at 95°C. The rabbit monoclonal antibodies against p-MAPK (Cell Signaling Technology, #4060, 0.5 μg/mL) or p-S6 (Cell Signaling Technology, #4858, 0.17 μg/mL) were applied for 60 minutes and detected with the Polymer Refine Detection Kit (Leica, DS9800). Antibody Leica Bond Polymer anti-rabbit HRP was used, followed by Refine Detection Kit Mixed DAB Refine for 10 minutes and Refine Detection Kit Hematoxylin counterstaining for 20 minutes. After staining, sample slides were washed in water, dehydrated using ethanol gradient (70%, 90%, and 100%), washed three times in HistoClear II (National Diagnostics, HS-202), and mounted in Permount (Fisher Scientific, SP15). For p16 IHC, samples were loaded into Leica Bond RX and pretreated with EDTA-based epitope retrieval ER2 solution (Leica, AR9640) for 20 minutes at 95°C. The mouse monoclonal antibody against p16 (Santa Cruz, sc-56330, 0.2 μg/mL) was applied for 60 minutes. Next Rabbit anti-mouse linker antibody (Leica Bond, Post Primary 1/5 dilution) and Leica Bond Polymer anti-rabbit HRP (Leica, DS9800) were used, followed by Refine Detection Kit Mixed DAB Refine for 10 minutes and Refine Detection Kit Hematoxylin counterstaining for 20 minutes. After staining, sample slides were washed in water, dehydrated using ethanol gradient (70%, 90%, and 100%), washed three times in HistoClear II (National Diagnostics, HS-202), and mounted in Permount (Fisher Scientific, SP15).

### Data Availability

The human sequence raw data generated in this study are protected and not publicly available due to patient privacy requirements but are available upon reasonable request from the corresponding authors subject to institutional approvals. Cell lines and patient tumor somatic mutations, identified by MSK-IMPACT sequencing, are available in the cBioPortal (https://www.cbioportal.org/study/summary?id=coadread_mskresistance_2022). All relevant cell-free DNA sequencing data are included within the article and supplementary data files.

## Authors' Disclosures

R. Yaeger reports grants and personal fees from Mirati Therapeutics and Array BioPharma/Pfizer, grants from Daiichi Sankyo and Boehringer Ingelheim, and personal fees from Natera and Zai Lab outside the submitted work. R. Mezzadra reports grants from the Cancer Research Institute during the conduct of the study. B. Weigelt reports grants from Repare Therapeutics outside the submitted work. M.F. Berger reports personal fees from Eli Lilly and AstraZeneca outside the submitted work. H. Der-Torossian reports other support from Mirati Therapeutics outside the submitted work. K. Anderes is an employee of Mirati Therapeutics. N.D. Socci reports grants from the NIH during the conduct of the study, as well as grants from the NIH outside the submitted work. J. Shia reports providing consulting services to Paige.AI. G.J. Riely reports grants from Mirati Therapeutics during the conduct of the study; grants from Lilly, Takeda, Merck, Roche, Pfizer, and Novartis outside the submitted work; and has been an uncompensated consultant for Daiichi Sankyo, Lilly, Pfizer, Merck, Verastem, Novartis, Flatiron Health, and Mirati Therapeutics. Y.R. Murciano-Goroff reports grants from the NCI/NIH during the conduct of the study; personal fees from AstraZeneca, Virology Education, and Projects in Knowledge (CME program with educational grant from Amgen), other support from Loxo Oncology at Eli Lilly, Elucida Oncology, Taiho Oncology, Hengrui USA/Jinagsu Hengrui Pharmaceuticals, Luzsana Biotechnology, Endeavor Biomedicines, Rutgers University Press, and Wolters Kluwer, grants from the NIH/NCI, Conquer Cancer, the ASCO Foundation (endowed by Dr. Charles M. and Carol A. Baum), and the Fiona and Stanley Druckenmiller Center for Lung Cancer Research outside the submitted work; and travel, accommodation, and expenses from AstraZeneca, honoraria from Virology Education and Projects in Knowledge (for a CME program funded by an educational grant from Amgen), associated research funding to the institution from Loxo Oncology at Eli Lilly, Elucida Oncology, Taiho Oncology, Hengrui USA/Jiangsu Hengrui Pharmaceuticals, Luzsana Biotechnology, and Endeavor Biomedicines, royalties from Rutgers University Press and Wolters Kluwer, training through an institutional K30 grant from the NIH (CTSA UL1TR00457), funding from a Kristina M. Day Young Investigator Award from Conquer Cancer, the ASCO Foundation, endowed by Dr. Charles M. Baum and Carol A. Baum, the Fiona and Stanley Druckenmiller Center for Lung Cancer Research, and a Paul Calabresi Career Development Award for Clinical Oncology (NIH/NCI K12 CA184746). B.T. Li reports grants and other support from Amgen and grants from the NIH during the conduct of the study; grants and personal fees from Hengrui USA, grants and other support from Genentech Roche, Lilly, AstraZeneca, and Daiichi Sankyo, nonfinancial support and other support from Resolution Bioscience, grants and nonfinancial support from

MORE Health, nonfinancial support from Jiangsu Hengrui Medicine, personal fees from Boehringer Ingelheim, and grants from the NIH outside the submitted work; and a patent for US62/685,057 issued, a patent for US62/514,661 issued, royalties from Karger Publishers, and licensing with Shanghai Jiao Tong University Press. J.G. Christensen reports personal fees from Mirati Therapeutics during the conduct of the study, as well as a patent for 10,633,381 issued, a patent for 10,689,377 issued, and a patent for 10,125,134 issued. J.S. Reis-Filho reports nonfinancial support and other support from Mission Bio during the conduct of the study, as well as personal fees from Goldman Sachs, Repare Therapeutics, Personalis, Volition RX, Grupo Oncoclinicas, Roche Tissue Diagnostics, MSD, Daiichi Sankyo, Paige.AI, and Bain Capital outside the submitted work. D.B. Solit reports personal fees from Pfizer, Vividion Therapeutics, BridgeBio, Fog Pharma, FORE Therapeutics, Scorpion Therapeutics, and Rain Therapeutics outside the submitted work. S.W. Lowe reports personal fees and other support from ORIC Pharmaceuticals and PMV Pharmaceuticals, and other support from Faeth Therapeutics, Blueprint Medicines, Senescea, and Mirimus, Inc. outside the submitted work, and that the laboratory receives financial support from Calico. N. Rosen reports grants and personal fees from AstraZeneca during the conduct of the study; personal fees and other support from MAPCure and Beigene, grants from Revolutionary Medicines, Pfizer-Colorado, and Boehringer Ingelheim, other support from Kura and Effector, and personal fees from Jubilant, Ikena, and Chugai outside the submitted work; a patent for a cream or lotion containing a standard RAF inhibitor to prevent the rashes induced by inhibitors of MEK, ERK, EGFR, and other inhibitors that inhibit ERK signaling in skin pending to Lutris; and work with biotech companies that is not relevant to the submitted work: Ribon (scientific advisory board and equity), ZaiLabs (scientific advisory board and equity), Concarlo (consulting), and Fortress (equity). S. Misale reports grants from Boehringer Ingelheim and Daiichi Sankyo outside the submitted work. No disclosures were reported by the other authors.

## Disclaimer

This research is the responsibility of the authors and does not necessarily represent the official views of the NIH.

## Authors' Contributions

**R. Yaeger**: Conceptualization, resources, data curation, formal analysis, supervision, funding acquisition, validation, methodology, writing–original draft, writing–review and editing. **R. Mezzadra**: Conceptualization, data curation, investigation, methodology, writing–review and editing. **J. Sinopoli:** Formal analysis, methodology. **Y. Bian:** Data curation, formal analysis, investigation, methodology. **M. Marasco:** Data curation, formal analysis, investigation, methodology, writing–review and editing. **E. Kaplun:** Formal analysis. **Y. Gao:** Formal analysis. **H. Zhao:** Formal analysis. **A. Da Cruz Paula:** Data curation, formal analysis, methodology. **Y. Zhu:** Data curation, formal analysis, visualization. **A. Chaves Perez:** Data curation, formal analysis, visualization. **K. Chadalavada:** Resources, formal analysis, validation, visualization, methodology. **E. Tse:** Data curation, formal analysis. **S. Chowdhry:** Data curation, formal analysis, methodology. **S. Bowker:** Resources, formal analysis, methodology. **Q. Chang:** Resources, formal analysis, visualization. **B. Qeriqi:** Resources, formal analysis, visualization. **B. Weigelt:** Resources, formal analysis, validation, methodology. **G.J. Nanjangud:** Resources, formal analysis, validation, methodology. **M.F. Berger:** Resources, formal analysis, validation, methodology. **H. Der-Torossian:** Resources, formal analysis. **K. Anderes:** Resources, formal analysis. **N.D. Socci:** Resources, formal analysis, validation, methodology. **J. Shia:** Resources, formal analysis, validation, methodology. **G.J. Riely:** Supervision. **Y.R. Murciano-Goroff:** Supervision. **B.T. Li:** Supervision. **J.G. Christensen:** Supervision. **J.S. Reis-Filho:** Supervision. **D.B. Solit:** Supervision. **E. de Stanchina:** Resources, supervision. **S.W. Lowe:** Conceptualization, resources, supervision, writing–review and editing. **N. Rosen:** Resources, supervision, writing–review and editing. **S. Misale:** Conceptualization, resources, data curation, formal analysis, supervision, validation, investigation, visualization, methodology, writing–original draft, writing–review and editing.

## Acknowledgments

This study was supported by NIH R01 CA233736 (R. Yaeger and N. Rosen), U54 OD020355 (E. de Stanchina), and Cancer Center Core Grant P30 CA008748. R. Mezzadra is a Cancer Research Institute Irvington Fellow supported by the Cancer Research Institute (CRI Award 3441). Y.R. Murciano-Goroff is supported by the Kristina M. Day Young Investigator Award from Conquer Cancer and the ASCO Foundation, and received training through an NIH K30 institutional grant (CTSA UL1TR00457).

## Note

Supplementary data for this article are available at Cancer Discovery Online (http://cancerdiscovery.aacrjournals.org/).

Received April 14, 2022; revised September 3, 2022; accepted November 9, 2022; published first November 10, 2022.

## REFERENCES

1. Zehir A, Benayed R, Shah RH, Syed A, Middha S, Kim HR, et al. Mutational landscape of metastatic cancer revealed from prospective clinical sequencing of 10,000 patients. Nat Med 2017;23:703–13.
2. Ostrem JM, Peters U, Sos ML, Wells JA, Shokat KM. K-Ras(G12C) inhibitors allosterically control GTP affinity and effector interactions. Nature 2013;503:548–51.
3. Lito P, Solomon M, Li LS, Hansen R, Rosen N. Allele-specific inhibitors inactivate mutant KRAS G12C by a trapping mechanism. Science 2016;351:604–8.
4. Skoulidis F, Li BT, Dy GK, Price TJ, Falchook GS, Wolf J, et al. Sotorasib for lung cancers with KRAS p.G12C mutation. N Engl J Med 2021;384:2371–81.
5. Ou SI, Janne PA, Leal TA, Rybkin II, Sabari JK, Barve MA, et al. First-in-human phase I/IB dose-finding study of adagrasib (MRTX849) in patients with advanced KRAS(G12C) solid tumors (KRYSTAL-1). J Clin Oncol 2022;40:2530–8.
6. Amodio V, Yaeger R, Arcella P, Cancelliere C, Lamba S, Lorenzato A, et al. EGFR blockade reverts resistance to KRAS. Cancer Discov 2020; 10:1129–39.
7. Fakih MG, Kopetz S, Kuboki Y, Kim TW, Munster PN, Krauss JC, et al. Sotorasib for previously treated colorectal cancers with KRAS(G12C) mutation (CodeBreaK100): a prespecified analysis of a single-arm, phase 2 trial. Lancet Oncol 2022;23:115–24.
8. Fakih M, Falchook GS, Hong DS, Yaeger RD, Chan E, Mather O, et al. CodeBreaK 101 subprotocol H: phase Ib study evaluating combination of sotorasib (Soto), a KRASG12C inhibitor, and panitumumab (PMab), an EGFR inhibitor, in advanced KRAS p.G12C-mutated colorectal cancer (CRC). Ann Oncol 2021;32 Suppl 5:S551. Abstract nr 434P.
9. Weiss J, Yaeger RD, Johnson ML, Spira A, Klempner SJ, Barve MA, et al. KRYSTAL-1: adagrasib (MRTX849) as monotherapy or combined with cetuximab (Cetux) in patients (Pts) with colorectal cancer (CRC) harboring a KRASG12C mutation. Ann Oncol 2021; 32 Suppl 5:S1294. Abstract nr LBA6.
10. Tanaka N, Lin JJ, Li C, Ryan MB, Zhang J, Kiedrowski LA, et al. Clinical acquired resistance to KRAS. Cancer Discov 2021;11:1913–22.
11. Awad MM, Liu S, Rybkin II, Arbour KC, Dilly J, Zhu VW, et al. Acquired resistance to KRAS G12C inhibition in cancer. N Engl J Med 2021;384:2382–93.
12. Zhao Y, Murciano-Goroff YR, Xue JY, Ang A, Lucas J, Mai TT, et al. Diverse alterations associated with resistance to KRAS(G12C) inhibition. Nature 2021;599:679–83.

13. Cheng DT, Mitchell TN, Zehir A, Shah RH, Benayed R, Syed A, et al. Memorial Sloan Kettering-Integrated Mutation Profiling of Actionable Cancer Targets (MSK-IMPACT): a hybridization capture-based next-generation sequencing clinical assay for solid tumor molecular oncology. J Mol Diagn 2015;17:251–64.
14. Serrano M, Lin AW, McCurrach ME, Beach D, Lowe SW. Oncogenic ras provokes premature cell senescence associated with accumulation of p53 and p16INK4a. Cell 1997;88:593–602.
15. Saoudaoui S, Bernard M, Cardin GB, Malaquin N, Christopoulos A, Rodier F. mTOR as a senescence manipulation target: A forked road. Adv Cancer Res 2021;150:335–63.
16. Sharpless NE, Sherr CJ. Forging a signature of in vivo senescence. Nat Rev Cancer 2015;15:397–408.
17. Collado M, Serrano M. The power and the promise of oncogene-induced senescence markers. Nat Rev Cancer 2006;6:472–6.
18. Ruscetti M, Leibold J, Bott MJ, Fennell M, Kulick A, Salgado NR, et al. NK cell-mediated cytotoxicity contributes to tumor control by a cytostatic drug combination. Science 2018;362:1416–22.
19. Lin AW, Barradas M, Stone JC, van Aelst L, Serrano M, Lowe SW. Premature senescence involving p53 and p16 is activated in response to constitutive MEK/MAPK mitogenic signaling. Genes Dev 1998;12:3008–19.
20. Wang C, Vegna S, Jin H, Benedict B, Lieftink C, Ramirez C, et al. Inducing and exploiting vulnerabilities for the treatment of liver cancer. Nature 2019;574:268–72.
21. Zhu Y, Tchkonia T, Fuhrmann-Stroissnigg H, Dai HM, Ling YY, Stout MB, et al. Identification of a novel senolytic agent, navitoclax, targeting the Bcl-2 family of anti-apoptotic factors. Aging Cell 2016;15:428–35.
22. Strickler JH, Loree JM, Ahronian LG, Parikh AR, Niedzwiecki D, Pereira AAL, et al. Genomic landscape of cell-free DNA in patients with colorectal cancer. Cancer Discov 2018;8:164–73.
23. Chan JM, Quintanal-Villalonga A, Gao VR, Xie Y, Allaj V, Chaudhary O, et al. Signatures of plasticity, metastasis, and immunosuppression in an atlas of human small cell lung cancer. Cancer Cell 2021;39:1479–96.
24. Russo M, Crisafulli G, Sogari A, Reilly NM, Arena S, Lamba S, et al. Adaptive mutability of colorectal cancers in response to targeted therapies. Science 2019;366:1473–80.
25. Thakur MD, Salangsang F, Landman AS, Sellers WR, Pryer NK, Levesque MP, et al. Modelling vemurafenib resistance in melanoma reveals a strategy to forestall drug resistance. Nature 2013;494:251–5.
26. Gonzalez-Cao M, Mayo de Las Casas C, Oramas J, Berciano-Guerrero MA, de la Cruz L, Cerezuela P, et al. Intermittent BRAF inhibition in advanced BRAF mutated melanoma results of a phase II randomized trial. Nat Commun 2021;12:7008.
27. Cayo A, Segovia R, Venturini W, Moore-Carrasco R, Valenzuela C, Brown N. mTOR activity and autophagy in senescent cells, a complex partnership. Int J Mol Sci 2021;22.
28. Kirkland JL, Tchkonia T. Senolytic drugs: from discovery to translation. J Intern Med 2020;288:518–36.
29. Gasek NS, Kuchel GA, Kirkland JL, Xu M. Strategies for targeting senescent cells in human disease. Nat Aging 2021;1:870–9.
30. Xue W, Zender L, Miething C, Dickins RA, Hernando E, Krizhanovsky V, et al. Senescence and tumour clearance is triggered by p53 restoration in murine liver carcinomas. Nature 2007;445:656–60.
31. Kang TW, Yevsa T, Woller N, Hoenicke L, Wuestefeld T, Dauch D, et al. Senescence surveillance of pre-malignant hepatocytes limits liver cancer development. Nature 2011;479:547–51.
32. Kale A, Sharma A, Stolzing A, Desprez PY, Campisi J. Role of immune cells in the removal of deleterious senescent cells. Immun Ageing 2020;17:16.
33. Amor C, Feucht J, Leibold J, Ho YJ, Zhu C, Alonso-Curbelo D, et al. Senolytic CAR T cells reverse senescence-associated pathologies. Nature 2020;583:127–32.
34. Zill OA, Banks KC, Fairclough SR, Mortimer SA, Vowles JV, Mokhtari R, et al. The landscape of actionable genomic alterations in cell-free circulating tumor DNA from 21,807 advanced cancer patients. Clin Cancer Res 2018;24:3528–38.
35. Odegaard JI, Vincent JJ, Mortimer S, Vowles JV, Ulrich BC, Banks KC, et al. Validation of a plasma-based comprehensive cancer genotyping assay utilizing orthogonal tissue- and plasma-based methodologies. Clin Cancer Res 2018;24:3539–49.
36. Shen R, Seshan VE. FACETS: allele-specific copy number and clonal heterogeneity analysis tool for high-throughput DNA sequencing. Nucleic Acids Res 2016;44:e131.
37. Carter SL, Cibulskis K, Helman E, McKenna A, Shen H, Zack T, et al. Absolute quantification of somatic DNA alterations in human cancer. Nat Biotechnol 2012;30:413–21.
38. Da Cruz Paula A, da Silva EM, Segura SE, Pareja F, Bi R, Selenica P, et al. Genomic profiling of primary and recurrent adult granulosa cell tumors of the ovary. Mod Pathol 2020;33:1606–17.
39. Schwarz RF, Trinh A, Sipos B, Brenton JD, Goldman N, Markowetz F. Phylogenetic quantification of intra-tumour heterogeneity. PLoS Comput Biol 2014;10:e1003535.
40. Pellegrino M, Sciambi A, Treusch S, Durruthy-Durruthy R, Gokhale K, Jacob J, et al. High-throughput single-cell DNA sequencing of acute myeloid leukemia tumors with droplet microfluidics. Genome Res 2018;28:1345–52.
41. Martin M. Cutadapt removes adapter sequences from high-throughput sequencing reads. EMBnet J 2011;17:10–2.
42. Li H, Durbin R. Fast and accurate short read alignment with Burrows-Wheeler transform. Bioinformatics 2009;25:1754–60.
43. Li H, Handsaker B, Wysoker A, Fennell T, Ruan J, Homer N, et al. The sequence Alignment/Map format and SAMtools. Bioinformatics 2009;25:2078–9.
44. McKenna A, Hanna M, Banks E, Sivachenko A, Cibulskis K, Kernytsky A, et al. The Genome Analysis Toolkit: a MapReduce framework for analyzing next-generation DNA sequencing data. Genome Res 2010;20:1297–303.
45. Poplin R, Ruano-Rubio V, DePristo MA, Fennell TJ, Carneiro MO, Van der Auwera GA, et al. Scaling accurate genetic variant discovery to tens of thousands of samples. bioRxiv 2018:201178.
46. Benjamin D, Sato T, Cibulskis K, Getz G, Stewart C, Lichtenstein L. Calling somatic SNVs and indels with Mutect2. BioRxiv 861054 [Preprint]. 2019. Available from: https://doi.org/10.1101/861054.
47. Weber LL, Sashittal P, El-Kebir M. doubletD: detecting doublets in single-cell DNA sequencing data. Bioinformatics 2021;37:i214–i21.
48. Demaree B, Delley CL, Vasudevan HN, Peretz CAC, Ruff D, Smith CC, et al. Joint profiling of DNA and proteins in single cells to dissect genotype-phenotype associations in leukemia. Nat Commun 2021;12:1583.
49. Alberti-Servera L, Demeyer S, Govaerts I, Swings T, De Bie J, Gielen O, et al. Single-cell DNA amplicon sequencing reveals clonal heterogeneity and evolution in T-cell acute lymphoblastic leukemia. Blood 2021;137:801–11.
50. Miller CA, McMichael J, Dang HX, Maher CA, Ding L, Ley TJ, et al. Visualizing tumor evolution with the fishplot package for R. BMC Genomics 2016;17:880.
51. Paula ADC, Zhu Y, Bhaloo SI, Pareja F, Hoang T, Selenica P, et al. Single-cell DNA sequencing from frozen endometrial tumors to address clonal evolution of somatic mutations. [abstract]. In: Proceedings of the American Association for Cancer Research Annual Meeting 2022; 2022 Apr 8–13. Philadelphia (PA): AACR; Cancer Res 2022;82(12_Suppl):Abstract nr 1692.
52. van Dijk D, Sharma R, Nainys J, Yim K, Kathail P, Carr AJ, et al. Recovering gene interactions from single-cell data using data diffusion. Cell 2018;174:716–29.